Hydrophobic Distal Pocket Affects NO−Heme Geminate Recombination Dynamics in Dehaloperoxidase and H64V Myoglobin

Stefan Franzen,*,† Audrius Jasaitis,‡,⊥ Jennifer Belyea,† Scott H. Brewer,† Robin Casey,† Alexander W. MacFarlane IV,§,∥ Robert J. Stanley,§ Marten H. Vos,‡ and Jean-Louis Martin‡

Department of Chemistry, North Carolina State University, Raleigh, North Carolina 27695, CNRS, UMR 7645, Laboratory for Optical Biosciences, Ecole Polytechnique, Palaiseau, France and INSERM U696, Palaiseau Cedex, France, and Department of Chemistry, Temple University, Philadelphia, Pennsylvania 19122

Received: November 23, 2005; In Final Form: May 10, 2006

The recombination dynamics of NO with dehaloperoxidase (DHP) from *Amphitrite ornata* following photolysis were measured by femtosecond time-resolved absorption spectroscopy. Singular value decomposition (SVD) analysis reveals two important basis spectra. The first SVD basis spectrum reports on the population of photolyzed NO molecules and has the appearance of the equilibrium difference spectrum between the deoxy and NO forms of DHP. The first basis time course has two kinetic components with time constants of $\tau_{11} \approx$ 9 ps and $\tau_{12} \approx 50$ ps that correspond to geminate recombination. The fast geminate process τ_{11} arises from a contact pair with the heme iron in a bound state with $S = 3/2$ spin. The slow geminate process τ_{12} corresponds to the recombination from a more remote docking site >3 Å from the heme iron with the greater barrier corresponding to a $S = 5/2$ spin state. The second SVD basis spectrum represents a time-dependent Soret band shift indicative of heme photophysical processes and protein relaxation with time constants of $\tau_{21} \approx 3$ ps and $\tau_{22} \approx 17$ ps, respectively. A comparison between the more rapid rate constant of the slow geminate phase in DHP−NO and horse heart myoglobin (HHMbNO) or sperm whale myoglobin (SWMbNO) suggests that protein interactions with photolyzed NO are weaker in DHP than in the wild-type MbNOs, consistent with the hydrophobic distal pocket of DHP. The slower protein relaxation rate τ_{22} in DHP−NO relative to HHMbNO implies less effective trapping in the docking site of the distal pocket and is consistent with a greater yield for the fast geminate process. The trends observed for DHP−NO also hold for the H64V mutant of SWMb (H64V MbNO), consistent with a more hydrophobic distal pocket for that protein as well. We examine the influence of solution viscosity on NO recombination by varying the glycerol content in the range from 0% to 90% (v/v). The dominant effect of increasing viscosity is the increase of the rate of the slow geminate process, τ_{12}, coupled with a population decrease of the slow geminate component. Both phenomena are similar to the effect of viscosity on wild-type Mb due to slowing of protein relaxation resulting from an increased solution viscosity and protein surface dehydration.

Introduction

The heme enzyme dehaloperoxidase (DHP) is the first globin known to have specific peroxidase activity. DHP was first isolated from the terebellid polychaete *Amphitrite ornata* and has recently been expressed in *E. coli*.[2] DHP has several interesting features that make it a key protein for studying dynamics in the context of enzyme function. First, the similarity of the spectroscopic bands and structure facilitates analogies between DHP and the extensively studied oxygen carrier globins myoglobin (Mb) and hemoglobin (Hb).[3] Second, the substrate binding pocket is adjacent to the distal heme pocket,[4,5] providing a key method for mapping dynamics near an enzyme substrate binding site using the same observables as have been used for more than 40 years to probe the distal pockets of Mb and Hb. Third, there is an interesting dynamic feature in DHP that resembles Mb, namely, there is a mobile histidine H55 (called the shuttle histidine) that can exist inside or outside the distal pocket analogous to the well-known behavior of the distal histidine of Mb.[4,5] Figure 1 shows the H55 residue in DHP and the equivalent H64 residue in sperm whale Mb. H64 in sperm whale myoglobin (SWMb) has been shown to have a pH-dependent conformation.[6,7] H64 points into the heme pocket at high pH and is surface/solvent exposed at low pH. In the DHP X-ray structure, H55 is also observed in two conformations that are analogous to the closed (heme pocket) and open (solvent-exposed) conformations in SWMb.[7−10] The overall secondary structures of DHP and SWMb are very similar, but the DHP protein fold is shifted by ∼1.5 Å with respect to the heme. Despite these similarities in structure and dynamics between SWMb and DHP, the heme is more deeply buried in the globin in DHP, so that the amino acid closest to the heme is V59 (corresponding to V68 in Mb). In SWMb, the closest amino acid residue is H64 (corresponding to H55 in DHP).[4,5,11,12] In the present study, we use NO recombination and viscosity/hydration effects to probe the consequence of these structural differences on the distal pocket dynamics of DHP. The H64V mutant of Mb provides an interesting comparison to DHP.

* To whom correspondence should be addressed. Fax: (919)-515-8920. E-mail: Stefan_Franzen@ncsu.edu.
† North Carolina State University.
‡ CNRS/INSERM.
§ Temple University.
⊥ Current address: Institut de Biologie Physico-Chimique, UMR 7141 CNRS/University Paris VI, 13 rue Pierre et Marie Curie, 75005 Paris, France.
∥ Current address: Fox Chase Cancer Center, 333 Cottman Avenue, Philadelphia, Pennsylvania 19111-2497.

10.1021/jp056790m CCC: $33.50
Published on Web 07/06/2006

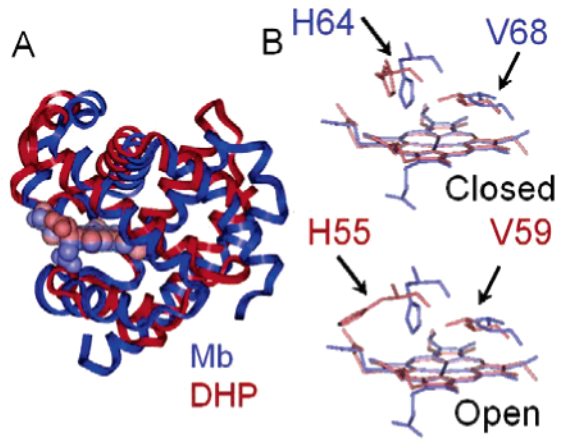

Figure 1. DHP and Mb structural superposition using the heme ring atoms as the common atoms. A high-resolution SWMb X-ray structure[95] and the DHP structure 1EW6[4] were retrieved from the Protein Data Bank. The superposition was carried out using InsightII (Accelrys, Inc.). (A) The similarity of the helical structure of DHP and Mb is shown; however, an offset of 1.5 Å relative to the heme ring atoms is shown. (B) The similarity of the residues in the distal pocket is shown. In the closed conformation both the valine and histine residues are present in the same relative orientation; however, the corresponding residues (Mb-H64/DHP-H55) and (Mb-V68/DHP-V59) are shifted by 1.5 Å relative to the heme iron. In the open conformation, DHP-H55 is in a solvent-exposed conformation 9 Å from the heme iron.

Replacement of H64 by a valine residue affects the closest contact with both bound and photolyzed NO. As shown in this study, the H64V mutant permits comparison of the histidine and valine interaction potential with photolyzed NO. Moreover, recombination of photolyzed NO in H64V MbNO shows an interesting similarity with DHP−NO recombination.

NO recombination with heme iron in heme enzymes has been studied previously to investigate the functional consequences of NO deligation in cytochrome *c* oxidase,[13] NO synthase,[14] and guanylate cyclase.[15] It is of great interest to compare the observed NO recombination dynamics in a globin enzyme to the extensive studies of Mb because of the large amount of information available in Mb from time-resolved studies of mutants, molecular dynamics simulations, and X-ray structural data that include time-resolved studies of the ligand trajectory. In principle, DHP provides a unique bridge from studies of Mb diatomic ligand binding trajectories to the dynamics (perhaps coupled dynamics) of cosubstrates (oxygen or peroxide) and the native substrate, 2,4,6-tribromophenol.[2] In this report, we compare the reported NO rebinding dynamics on the picosecond time scale in nitroxy myoglobin (MbNO) with those in DHP−NO and the H64V MbNO mutant of Mb. The crystal structure of the H64V mutant reveals that valine is the closest amino acid to the heme iron, thus creating a distal pocket that more closely resembles that of DHP.[16] Thus, the present study is a comparison of the ligand dynamics in the distal pocket of two different proteins (H64V MbNO and DHP−NO), which both have a distal valine as the closest amino acid to the bound NO ligand. The similarity of the spectral features reveals a novel aspect of the dynamics that will provide an understanding of the electrostatic and conformation environment of the distal pocket in both globins and peroxidases.

The recombination of small diatomic ligands with the heme prosthetic group in Mb following photolysis has served as a model reaction for the study of protein dynamics for many decades.[17−20] The rebinding of diatomic ligands, such as CO, NO, or O_2, is strongly coupled to motions of the protein through electrostatic interactions with amino acid side chains in the distal pocket.[21,22] Analysis of the potential-energy surfaces calculated using density functional theory methods suggests that the time scales for ligand recombination depend on the spin state of bound and photolyzed CO, NO, or O_2 ligand.[23] In the case of CO, there are two distinct phases of ligand rebinding. The faster geminate (i.e., involving rebinding of photolyzed CO molecules prior to their escape from the protein into the solvent) phase occurs with a ∼4% yield on the submicrosecond time scale in room-temperature solutions.[20] The slower bimolecular phase involves the recombination of CO molecules after their escape into solution and occurs on the millisecond time scale for the protein and CO concentrations normally studied. The recombination of CO is quite slow compared to NO or O_2. This difference can be understood in terms of the forbidden nature of the transition from the $S = 2$ photolyzed species to the $S = 0$ six-coordinate ground state for CO recombination. Oxygen binding to Mb is significantly more complicated due to the presence of multiple spin states, and there is a paucity of data due to multiple time scales and difficulty of autoxidation.[24,25] NO has been the ligand of choice for studies of trajectories that can be compared with molecular dynamics since photolyzed NO in Mb exhibits rapid, large-amplitude ligand recombination on the picosecond time scale, has a near unity yield for geminate recombination, and is not subject to auto-oxidation difficulties.[1,14,26−29]

In this work, we examine how glycerol content of the buffer solution affects NO recombination to the heme in DHP and H64V Mb at room temperature. The study follows an earlier report on the effect of glycerol on NO recombination in HHMb.[1] The primary conclusion of that report was that upon photolysis at room temperature an immediate branching occurs, following which some fraction of the dissociated NO molecules recombine with a fast rate while the rest recombine with at least one, significantly slower, glycerol-concentration-dependent rate.[1] The slow process is temperature-dependent based on a recent study of the temperature dependence of NO recombination in Mb.[30] The origin of the branching is still under investigation. There are two rotamers of photolyzed NO in the heme pocket in cryogenic studies[31] and time-resolved infrared studies at room temperature.[32] A recent study of NO recombination in the V68W mutant of myoglobin[30] shows only the fast phase of NO recombination, essentially ruling out the role of the NO rotamers as the origin of two kinetic phases. The fast recombination phase has no temperature dependence and is therefore activationless. Phenomenologically, the temperature-dependent data support the role of the two possible spin states of a photolyzed NO ligand ($S = 5/2$ and $3/2$) that both recombine with the $S = 1/2$ ground state.[23,33] Similar observations in photolyzed CO myoglobin using a variety of methods show that the pathway for this diatomic into the docking site is blocked by the V68W mutation and that this eliminates ligand diffusion for CO.[34,35] While the character of the two kinetic phases is now much clearer due to recent studies,[1,30−32] the origin of the partitioning has not been determined. The time-resolved spectroscopic study of ligand recombination in photolyzed DHP−NO and H64V Mb−NO provides evidence for the key role of the distal histidine in stabilizing the NO ligand in the docking site. Stabilization in the docking site provides a barrier to recombination that is modulated by protein dynamics and temperature.[30]

Materials and Methods

Sample Preparation. The dehaloperoxidase gene from *Amphitrite ornata* has been cloned into a Rosetta cell line of *E. coli* and expressed at a high level.[2] Dehaloperoxidase (DHP) and the H64V mutant of SWMb (H64V) were expressed and

purified using methods described in detail elsewhere.[36] Horse heart Mb (HHMb) was purchased from Sigma. Dehaloperoxidase was dissolved in 50 mM phosphate buffer at pH 7.4, reduced with ascorbate, and exposed under oxygen-free conditions to 0.01 atm of NO. For some experiments, as noted, deoxygenated glycerol was added to the sample to obtain the desired volume/volume percentage of glycerol in buffer. The preparation of samples with varying glycerol content was performed by sequentially weighing the cuvette and then the added glycerol followed by the buffer solution containing the protein. The weights were converted to volume using the densities ρ(glycerol) = 1.26 g/cm^3 and ρ(water) = 1.00 g/cm^3. The procedure was the same as that used in an earlier study on HHMb.[26] The previous report referred to the glycerol percentages as weight-to-volume (w/v), which was technically not correct since the weights were converted to volumes using the density. A major effect of added glycerol was to increase the solvent viscosity (from ~1 cP in buffer to ~200 cP at 90% v/v glycerol[37]); however, glycerol addition was also capable of changing the internal hydration state of proteins.[38] After binding of NO, the DHP−NO sample was transferred under an argon atmosphere to a gastight sample cell (1 mm optical path) in which the experiments were performed. All experiments were performed at ambient laboratory temperature (21 ± 1 °C).

Experimental Procedures. Multicolor transient absorption pump−probe spectroscopy[39] was performed with a 30 fs pump pulse centered at 565 nm and a <30 fs white light continuum probe pulse at a repetition rate of 30 Hz. Full spectra of the test and reference beams were recorded using a combination of a polychromator and a CCD camera. All experiments were carried out at 21 ± 1 °C. Data were recorded up to 100 (DHP and H64V) or 300 ps (HHMb). In separate experiments time-resolved spectra as a function of glycerol concentration were measured using a 1 kHz Ti:sapphire-based regenerative amplified laser system as described in detail elsewhere.[40] For these experiments, the pump pulse was tuned to 400 nm and the probe wavelength, derived from a crystal quartz-generated white light continuum, was tuned as indicated below. The instrument response for these measurements was about 350 fs.

Data Analysis. Basic data matrix manipulations and presentation were done using IgorPro5.0. Singular value decomposition (SVD) and fits to a biexponential model were also performed using IgorPro5.0. The SVD transformation is $\mathbf{A}(\lambda,t) = \mathbf{U}(\lambda)\mathbf{W}\mathbf{V}^{T}(t)$, where the $\mathbf{U}(\lambda)$ matrix contains the basis spectra and the $\mathbf{V}^{T}(t)$ matrix contains the corresponding basis time courses. The **W** matrix contains the weighting that defines the magnitude of each basis spectrum in the original data set. The details of the SVD analysis and additional figures that complement those presented here are available in the Supporting Information. In all cases there were only two significant basis spectra based on the magnitude of the eigenvalues. The second SVD basis spectrum is approximately 10% of the magnitude of the first in all of the kinetic data sets studied. The third SVD basis spectrum has less than 2% of the magnitude of the first basis spectrum and was neglected in the analysis.

Examination of the basis time courses of the $\mathbf{V}^{T}$ matrix reveals that they are not pure kinetic components. $\mathbf{V}^{T}_1$ is mainly a population decay, and $\mathbf{V}^{T}_2$ is mainly a Soret band shift that reports on heme and protein relaxation following photolysis. The mixing of population decays and the Soret band has been observed on a 4 order of magnitude longer time scale in CO recombination studies.[41] A matrix rotation can be applied to give physically meaningful kinetic components following the established procedures.[41] The rotated $\mathbf{V}^{T}$ matrix is called the $\mathbf{S}^{T}$ matrix:

$$S_1^{T} = W_1 \cos(\theta)\, V_1^{T} + W_2 \sin(\theta)\, V_2^{T}$$

$$S_2 = -W_1 \sin(\theta)\, V_1^{T} + W_2 \cos(\theta)\, V_2^{T} \quad (1)$$

The corresponding rotated **U** matrix is called the **R** matrix:

$$R_1 = \cos(\theta)\, U_1 + \sin(\theta)\, U_2$$

$$R_2 = \sin(\theta)\, U_1 + \cos(\theta)\, U_2 \quad (2)$$

It was assumed that the Soret band shift occurred in a unique direction (which is evident in the raw data). Thus, mixing of the first SVD basis time course into the second gives rise to a small negative feature that can be removed by matrix rotation.[41] The angle $\theta = 10°$ applied to the rotation of all data sets is the minimum angle that gives an entirely positive decay in the second time course. The results presented below were all on the physically meaningful rotated matrixes. The deconstruction of the data matrix is $\mathbf{A}(\lambda,t) = \mathbf{R}(\lambda)\mathbf{S}^{T}(t)$ using the rotated matrixes. Note that the singular values W_i are incorporated in the $\mathbf{S}^{T}$ matrix.

Density Functional Theory Calculations. The model system used in this study consisted of an imidazole (Im), methane (CH_4), water (H_2O), or benzene (C_6H_6) molecule hydrogen bonded to NO in one of two geometries R−H···NO or R−H···ON. The optimized ground-state geometries and potential-energy surfaces of the hydrogen-bonding interaction were obtained using the GGA functional[42,43] as implemented in DMol3 (Accelrys Inc.).[44,45] All calculations were carried out on a PQS QuantumCube computer. Geometry optimizations were carried out without constraints until the energy difference was less than 10^{-6} au on subsequent iterations (Supporting Information). Numerically tabulated basis sets of double-ζ plus extra polarization (DNPP) quality were employed as described in the Supporting Information. For the DNPP basis there are four basis functions for H (1s, 2s, 2p, 3d) and seven basis functions for C, N, and O (1s, 2s(2), 2p(2), 3d, 4f). The potential-energy surfaces were calculated using the Thermal option (grand canonical ensemble) treatments of the density functional.[46] The grand canonical (Thermal) option always converged to a lower overall energy. The grand canonical calculation was carried out at an electronic temperature corresponding to $k_BT = 0.02$ Hartrees. Once a calculation was complete it was extrapolated to zero temperature by subtraction of the thermal electron occupation according to the grand canonical partition function.

Although carried out in a separate publication,[23] the spin-dependent model discussed in this study was developed by means of explicit potential-energy surfaces calculated using density functional theory (DFT) that include curve crossings of all possible spin states of the three common diatomic ligands CO, NO, and O_2 and high-spin heme iron. The NO ground state is spin 1/2, and the photolyzed states can have spin 3/2 or 5/2. The methods and level of theory for determining the interaction of NO with imidazole (histidine) and methane (valine) were the same as those used to determine the interaction with the heme iron.

Results

The equilibrium absorption spectrum of the ferrous unliganded form of dehaloperoxidase (DHP) (or any other protein binding *b*-type heme[47]) consists of weak Q-band absorptions in the 550 nm region and an intense Soret band absorption around 435 nm. The binding of NO to the heme causes a spectral shift of the Soret band to 420 nm. In the experiments described

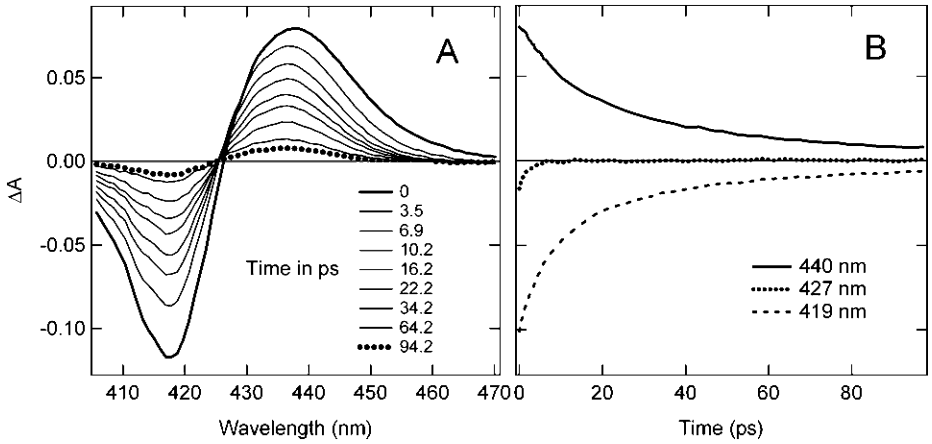

Figure 2. Selected time-resolved difference spectra and time courses corresponding to NO recombination from photolyzed DHP−NO. (A) Time-resolved difference spectra are shown at the indicated time in picoseconds. (B) Representative kinetic traces are shown at the indicated wavelengths.

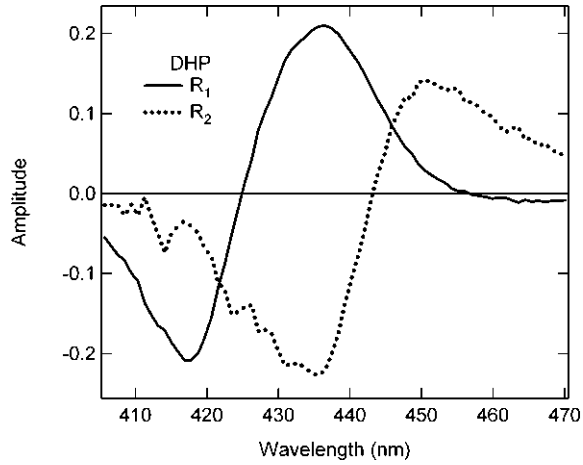

Figure 3. Spectral changes observed after photodissociation of the DHP−NO complex in buffer. Two *R*-matrix basis spectra are shown resulting from the rotated SVD analysis.

below we applied the pump−probe approach where we start with the NO-bound protein and excite it with a short laser pulse centered at 565 nm, resulting in NO photolysis. In the difference absorption spectrum (photolyzed minus unphotolyzed), this photolysis leads to a negative feature (bleach) near 420 nm and a positive feature (induced absorption) around 438 nm. The subsequent rebinding of NO to the heme on the picosecond time scale was monitored in the spectral range from 400 to 465 nm. Similar results were obtained using excitation at both 565 and 400 nm pump wavelengths. The influence of the solution viscosity (or possibly dehydration) on the NO recombination rate was studied by varying the glycerol content in the buffer. The kinetics of NO recombination to ferrous DHP and the H64V mutant of myoglobin at glycerol concentrations ranging from 0% to 90% (v/v) were investigated.

Figure 2 shows time-dependent spectra and kinetics at selected wavelengths obtained from the femtosecond flash photolysis experiment on DHP−NO. These data are representative of data obtained for DHP−NO photolysis in glycerol and for the H64V MbNO mutant data as well. Figure 3 shows the difference spectra corresponding to the two significant basis spectra from the SVD analysis of the data in Figure 2. Although 9 time points are shown in Figure 2, a total of 52 time points were used in the SVD analysis. In our analysis we will only report the rotated SVD basis time courses and spectra. This method is a legitimate means of reporting the SVD basis time courses since we have only formed linear combinations of known components. The first basis spectrum R_1 corresponds to the deoxy−NO Soret difference spectrum (negative ΔA corresponding to NO-bound heme at 420 nm and positive ΔA corresponding to deoxy-heme at 438 nm) and hence is proportional to the population of the photolyzed NO. The rotated basis time course S^T_1 corresponding to R_1 is shown in Figure 4A. The R_2 basis spectrum in Figure 3 (dotted line) corresponds to a band shift in the photolyzed deoxy Soret band that indicates a rapid electronic, vibrational, or structural relaxation that occurs following photolysis. The singular value of the R_2 basis spectrum is approximately 1/10 as large as that of R_1. The kinetic behavior of the R_2 basis spectrum of DHP−NO in buffer and 50% glycerol/buffer is shown as S^T_2 in Figure 4B.

The time-dependent spectra and time courses of photolyzed H64V MbNO are similar to those of DHP−NO as shown in Figure 5. The *R* basis spectra for H64V MbNO shown in Figure 6 have similar features to the DHP−NO data. We focus the analysis on the systematic differences in the kinetic components depending on protein and glycerol concentration. To aid in understanding the influence of the distal valine, V59, in DHP, we studied the NO binding properties in the H64V mutant form of myoglobin. As shown in the Supporting Information, the SVD basis spectra for NO binding in H64V Mb−NO are very similar to those of DHP−NO in all cases.

We turn our analysis to the different components of both the NO recombination and Soret band shift decay curves designated S^T_1 and S^T_2, respectively. The S^T_2 time courses shown in Figures 4 and 6 have been multiplied by 10, and thus there is a smaller signal-to-noise ratio in the S^T_2 component. The S^T_1 and S^T_2 kinetic data were fit as presented in Tables 1 and 2, respectively, to a biexponential model consisting of two rate constants k_{ij} with amplitudes A_{ij}, where i is the number of the basis time course and j is number of the exponential component. A detailed description of fits of the SVD time courses with combinations of fixed and free rate constant parameters are presented in the Supporting Information. The fits in the Supporting Information also use a baseline in addition to the two kinetic components to permit comparison with other published values. The kinetic components shown in Tables 1 and 2 have a systematic trend that the amplitude of the more rapid process increases with increasing glycerol content. Table 1 shows that the time constant of the more rapid process in S^T_1 is $\tau_{11} \approx 11$ ps in H64V MbNO and $\tau_{11} \approx 9$ ps in DHP−NO. The time constant of the rapid phase is quite similar for both DHP and H64V with the exception of DHP−NO in 90% glycerol/buffer where it is $\tau_{11\approx}$ 5.4 ps. Although the rate constant for the fast phase in H64V MbNO

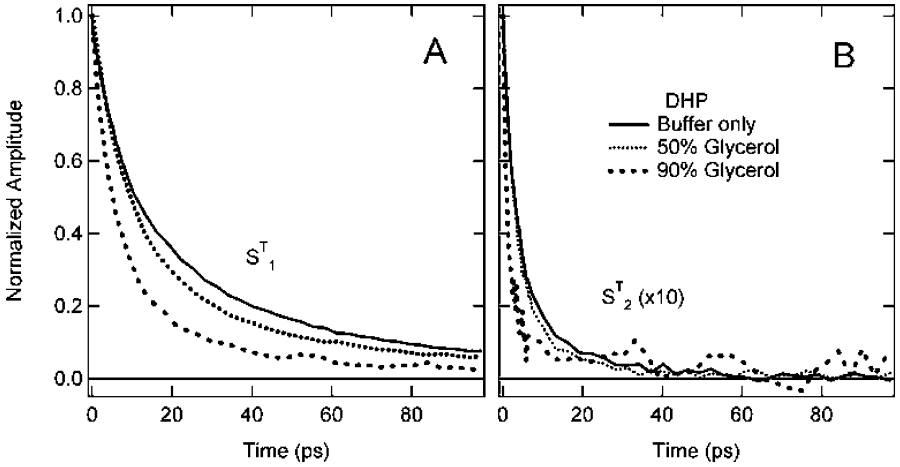

Figure 4. Kinetic time courses of NO rebinding in photolyzed DHP−NO. The S^T rotated basis time courses from the rotated $\mathbf{V^T}$ matrix were obtained by eq 1. (A) Time course S^T_1 represents NO rebinding. (B) Time course S^T_2 represents the deoxy Soret band shift in the photolyzed state.

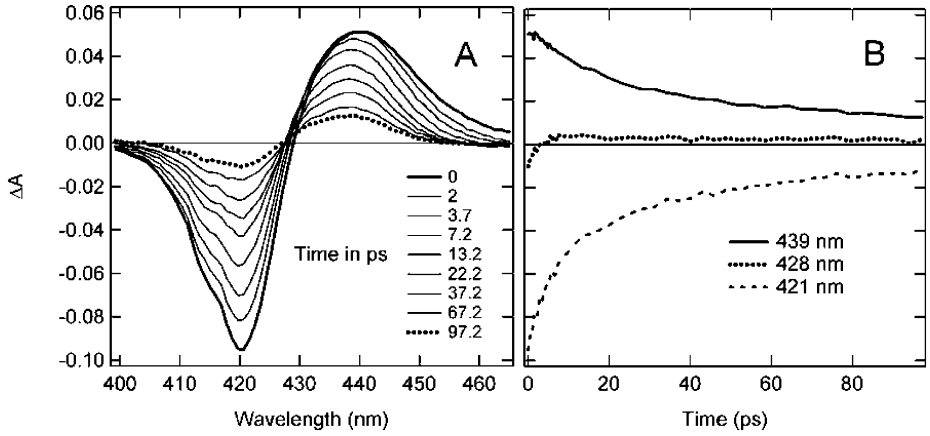

Figure 5. Selected time-resolved difference spectra and time courses corresponding to recombination of NO in photolyzed H64V MbNO. (A) Time-resolved difference spectra are shown at the indicated time in picoseconds. (B) Representative kinetic traces are shown at the indicated wavelengths.

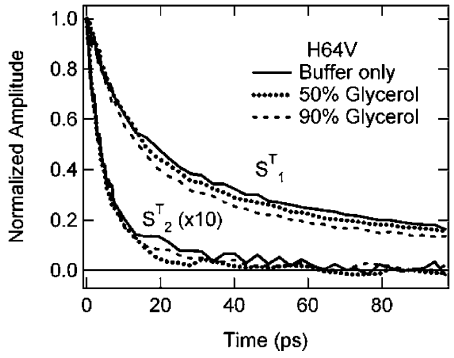

Figure 6. Kinetic components of NO rebinding in photolyzed H64V MbNO. The S^T rotated basis time courses of the rotated $\mathbf{V^T}$ matrix were obtained by eq 1. (A) Time course S^T_1 represents NO rebinding. (B) Time course S^T_2 represents the deoxy Soret band shift in the photolyzed state.

does not change by a large amount, the amplitude of the fast phase changes from 52% to 63% as the glycerol concentration is increased from 0% (pure buffer) and 90% glycerol/buffer. A similar trend is observed for DHP−NO with an increase in the amplitude of the fast component from 56% to 76%. DHP−NO in 90% glycerol/buffer shows an increase in the recombination rate constant of rapid phase. This trend in the amplitude of the fast and slow phase for recombination is analogous to the effect of glycerol concentration on the NO rebinding kinetics of HHMbNO.[1] The fast recombination process in HHMbNO has a lifetime of $\tau_{11} \approx 8.5$ ps, compared to average lifetimes of $\tau_{11} \approx 7.7$ ps and $\tau_{11} \approx 10.7$ ps for the DHP−NO and H64V MbNO samples, respectively. The slow geminate process has time constants of $\tau_{12} \approx 54$ ps and $\tau_{12} \approx 92$ ps in DHP−NO and H64V MbNO samples, respectively. Both of these time constants are significantly shorter than the time constant for HHMbNO ($\tau_{12} \approx 310$ ps), indicating that the geminate process from the docking site has a greater rate constant in DHP−NO and H64V MbNO compared to HHMbNO. The increase in the rate constant k_{12} and decrease in the yield of slower geminate process A_{12} as a function of increasing glycerol concentration is similar in all proteins studied.[1]

Analysis of S^T_2 provides information on the time scale of the electronic relaxation process on the heme as well as protein relaxation that follows ligand photodissociation. The dominant rapid phase in S^T_2 corresponds to well-known photophysical processes that have been observed in photolyzed heme proteins.[33,48−50] Inspection of Figures 4 and 6 and the corresponding fit parameters in Table 2 shows that the initial large kinetic component of S^T_2 associated with the deoxy Soret band shift τ_{21} has a 3−4 ps lifetime for all proteins except DHP−NO in 90% glycerol/buffer, which has an even shorter lifetime of 1.3 ps. This lifetime is significantly shorter than the most rapid phase of NO recombination (S^T_1). The fast component τ_{21} is largely independent of the nature of the protein or its solvation, consistent with a photophysical relaxation of the heme itself. The data are particularly striking in Figure 6, where the

TABLE 1: Fits of the Biexponential Model to S^T_1 Shown in Figures 4 and 6 for Photolyzed DHP−NO and H64V MbNO, Respectively[a]

parameter	H64V	H64V 50%	H64V 90%	DHP	DHP 50%	DHP 90%	Mb
A_{11}	0.518 ± 0.018	0.594 ± 0.014	0.627 ± 0.014	0.562 ± 0.011	0.697 ± 0.010	0.761 ± 0.015	0.621 ± 0.00605
k_{11}(ps^{-1})	0.0960 ± 0.0050	0.0879 ± 0.0029	0.0910 ± 0.0029	0.113 ± 0.0026	0.114 ± 0.002	0.185 ± 0.0053	0.117 ± 0.0036
τ_{11} (ps)	10.4	11.4	10.3	8.8	8.8	5.4	8.5
A_{12}	0.482 ± 0.019	0.406 ± 0.015	0.373 ± 0.015	0.437 ± 0.011	0.312 ± 0.010	0.239 ± 0.015	0.379 ± 0.0050
k_{12} (ps^{-1})	0.0109 ± 0.00061	0.0103 ± 0.00053	0.0112 ± 0.00061	0.0190 ± 0.0004	0.0186 ± 0.00057	0.0261 ± 0.0016	0.00322 ± 0.0001
τ_{12} (ps)	91.7	97.0	89.3	52.6	53.7	38.3	310[b]

[a] The data shown in the figures are normalized, and the components below are also normalized. The percentages given in each column refer to the percent glycerol content of the sample. [b] The time constant measured here for HHMbNO is longer than most reports, likely because of the 100 ps data acquisition. Typical lifetimes for NO recombination in myoglobins are ~200 ps[1]. Given that the focus of this study is DHP and the H64V mutant, we included these data for comparison under the conditions of the experiment.

TABLE 2: Fits of the Biexponential Model to S^T_2 Shown in Figures 4 and 6 for Photolyzed DHP−NO and H64V MbNO, Respectively[a]

parameter	H64V	H64V 50%	H64V 90%	DHP	DHP 50%	DHP 90%	Mb
A_{21}	0.755 ± 0.033	0.789 ± 0.054	0.803 ± 0.029	0.738 ± 0.021	0.828 ± 0.024	0.873 ± 0.032	0.529 ± 0.033
k_{21} (ps^{-1})	0.261 ± 0.017	0.258 ± 0.017	0.254 ± 0.012	0.322 ± 0.012	0.319 ± 0.013	0.79012 ± 0.0654	0.618 ± 0.048
τ_{21} (ps)	3.8	3.9	3.9	3.1	3.1	1.3	1.6
A_{22}	0.244 ± 0.035	0.211 ± 0.057	0.197 ± 0.030	0.252 ± 0.022	0.172 ± 0.026	0.127 ± 0.018	0.473 ± 0.032
k_{22} (ps^{-1})	0.0398 ± 0.0051	0.0666 ± 0.012	0.0455 ± 0.0058	0.0598 ± 0.0043	0.0570 ± 0.007	0.0252 ± 0.0067	0.105 ± 0.0073
τ_{22} (ps)	25.1	15.0	22.0	16.7	17.5	39.7	9.5

[a] The data shown in the figures are normalized, and the components below are also normalized. The percentages given in each column refer to the percent glycerol content of the sample.

first 4 ps are essentially superimposable, while there is a noisy difference on the longer time scales of the S^T_2 basis time course. These fluctuations of nearly 10% in the signal of S^T_2 (×10) reflect the 100:1 signal-to-noise ratio of the data set. There may be a systematic difference of the slower component τ_{22} with a time constant that varies in the range $\tau_{22} \approx 15-40$ ps. Although relatively small, the τ_{22} component of the Soret band shift reports on the relaxation of the protein around the photolyzed NO ligand. The key point is that this component has a time constant that is intermediate between the two components of S^T_1, i.e., $\tau_{11} < \tau_{22} < \tau_{12}$. Protein relaxation with rate constant k_{22} likely plays a key role in determining the partitioning among the different geminate recombination channels k_{11} and k_{12}. The matrix rotation analysis would give a slightly different interpretation if the angle were altered. If a smaller θ angle were used in eq 1, S^T_2 would have a negative feature and be fit by more than two exponentials (see Supporting Information). If a larger θ angle were used in eq 1, the kinetics of S^T_2 would more closely resemble the population decay S^T_1 and the 15−40 ps kinetic component would become a smaller part of a more complex multiexponential decay. The overall conclusion that there is a kinetic component that is intermediate between the fast and slow phases of S^T_1 that would not be changed by the change in angle, but the kinetic fits would be more complicated.

On the basis of the fits to the population time course S^T_1 the slow component shows a systematic difference between the globins with a distal valine and a distal histidine as the closest amino acid side chain to bound NO. Although valine is generally not considered to be involved in hydrogen bonding, we hypothesize that the interaction potential of the closest distal residue affects the binding of photolyzed NO in the docking site. By analogy with the imidazole ring, we will refer to this as a hydrogen bond as has been done for similar systems[51−53] and in a recent study of similar interactions between CO and distal residues in photolyzed SWMbCO.[54] The more rapid recombination in the globins with a distal valine may depend on the strength of the interaction of NO with the amino acid side chain. To estimate the strength of this interaction potential, we performed density functional theory (DFT) calculations to examine the hydrogen-bonding interaction of methane and imidazole with NO. These two molecules represent the side chains of valine and histidine, respectively. The binding interaction was calculated for each of two different orientations of NO possible in the distal pocket. The point of these calculations is to determine whether the distal side chain interaction could give rise to two populations of NO molecules in the docking site. The calculations were carried out on R−H···NO and R−H···ON, where R = $C_3N_2H_3$ (Im), CH_3, HO, and C_6H_5. Water and benzene were included in the calculation for comparison (see Supporting Information). The potential-energy surfaces are presented in Figure 7. The strongest interaction is Im−H···NO, which has a potential energy of ~3 kJ/mol. By contrast H_2O, C_6H_6, and CH_4 all have interaction potential energies of ~1 kJ/mol. The difference in interaction potentials may affect the residence time of NO in the distal pocket as discussed below.

Discussion

DHP is the first known peroxidase with a globin fold, and thus it provides a model system that can be used to address questions regarding interaction of the substrate and the heme active site. The X-ray crystallographic data on DHP shows that the substrate binding pocket is adjacent to the distal pocket of the heme and in close proximity to the heme iron.[4,5] Despite the difference in function, the distal pocket of DHP in the vicinity of the heme iron is quite similar to that of Mb. Figure 1 shows that the major difference in the conformation of the two closest distal amino acid residues in DHP and SWMb is a 1.5 Å shift in position relative to the position of the heme. The similarity in distal pocket structure is surprising given that DHP is a peroxidase/globin and SWMb is a globin with little peroxidase activity.[2] One further difference between DHP and Mb is that the distal histidine, H55, in DHP exists in two fluctuating conformations in the X-ray crystal structure shown as the open and closed conformations in Figure 1. The distal histidine of Mb, H64, can also exist in two pH-dependent conformations; however, the available evidence suggests that H64 is protonated and solvent exposed at pH < 4.5.[7,8] Although the X-ray structure of DHP was determined at pH 6.5, the reported structure has

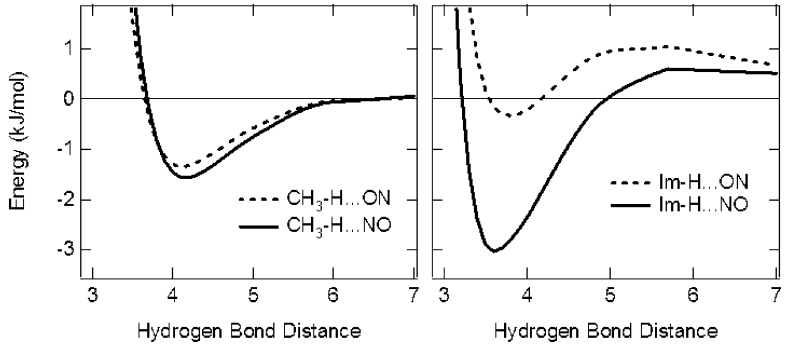

Figure 7. Comparison of the potential-energy surfaces for the nitric oxide interaction with methane and imidazole. Both orientations of nitric oxide are shown. The reference energy was assumed to be zero at 10 Å separation.

two H55 conformations of equal occupancy (Figure 1).[55] The conformational flexibility of the distal histidine in DHP is a key point for understanding substrate entry into the enzyme since the X-ray crystal structure with substrate bound has the distal histidine only in the solvent-exposed or open conformation. When DHP exists in the open conformation, the distal pocket is extremely hydrophobic with no polar residues within 9 Å of the heme iron (other than the propionate side chains of the heme itself). Experiments that probe NO recombination in Mb mutants have been interpreted in terms of the trajectory of NO ligands in the distal pocket. The goal of the present study is to understand the role played by the distal histidine in DHP with reference to the extensive data obtained from flash-photolysis studies of MbNO.

The dependence of NO recombination on glycerol, temperature, and distal pocket mutation in myoglobin has been studied by a number of groups.[1,27−30,32−34,56−59] Time-resolved NO rebinding studies provide a general probe of distal pocket structure in heme proteins.[14,60−65] Recombination of NO is non-single-exponential in nearly every heme protein studied. In a previous study of NO recombination in HHMb, a maximum entropy model was applied to the NO rebinding kinetics in the presence of varying glycerol concentrations.[1] The maximum entropy model is a bias-free method for determining the distribution of rate constants in a nonexponential kinetic trace. The maximum entropy method is consistent with a biexponential model as a fitting function for the kinetics of HHMbNO due to the exponential nature of NO rebinding to HHMbNO. When a baseline is included in the fitting it can represent a third slower kinetic component. This component is smaller for DHP−NO (<10%) and H64V MbNO (<5%) than it is for HHMbNO (<15%), as shown in the Supporting Information. On the basis of the previous results and the qualitative similarity in the data the biexponential model without a baseline was applied to fit the kinetics of both DHP−NO and H64V MbNO throughout the range of glycerol concentrations studied. The analysis of SWMbNO and HHMbNO kinetics led to the conclusion that on the time scale of a few hundred picoseconds, two kinetic processes describe NO rebinding.[1,14] For SWMbNO, one process is described with a time constant of ∼5 ps and the second corresponding to a time constant of ∼133 ps when the kinetics are fit to a biexponential model with no baseline.[32] HHMbNO recombination kinetics have been fit to a biexponential model with recombination times of ∼10 and ∼200 ps,[1,25] although here we obtain a slightly longer lifetime of ∼310 ps for the slow phase of HHMbNO as shown in Table 1. Since HHMbNO has the largest baseline, there is the greatest uncertainty in the fit to the rate constant for the slower component of HHMbNO.

Table 1 shows that the population term for NO recombination shows similar behavior in H64V MbNO and DHP−NO. The fast components in DHP−NO and H64V MbNO have lifetimes that are not significantly different from those of SWMbNO and HHMbNO. The lifetimes of the slower components are approximately $\tau_{12} \approx 54$ and 92 ps for DHP−NO and H64V MbNO, respectively, which are both significantly shorter than that of wild-type HHMbNO as shown in Table 1 and SWMbNO.[32] As observed in HHMbNO, the primary effect of increasing glycerol content is that the amplitude of the slower process is decreased along with a concomitant increase in its rate constant. The amplitude of the faster process increases with no significant change in rate constant as the glycerol content is increased. One conclusion of the present study is that the mutation of the distal residue from histidine to valine affects the dynamics of the slower process since a more hydrophobic distal pocket provides less stabilization for the photodissociated ligand. A second conclusion, consistent the X-ray crystal structure of DHP, is that H55 is not strongly interacting with the photodissociated NO ligand. By this we suggest that there is a significant conformation of the "open" conformation in which H55 is solvent exposed and not available for hydrogen bonding.

Table 2 gives the fit parameters for the two components of the S^T_2 SVD time courses, which correspond to the Soret band shift with respect to the equilibrium deoxy band in the difference spectra of the respective photolyzed species. The slower component of the band shift is attributed to protein relaxation in the distal pocket. The faster component arises from relaxation of the heme itself, and in previous studies we hypothesized that this component arises from transient trapping of the heme iron in a mixed spin state which relaxes on the time scale of ∼3−4 ps.[50] The slower component of the band shift is attributable to the relaxation of amino acid side chains in the distal pocket around photolyzed NO. Similar perturbations have been observed upon photodissociation of NO from the heme domains of the sensors FixL[66] and *Ec*Dos,[67] where they were suggested to be associated with intermediates in the allosteric intraprotein signaling pathway. The SVD analysis reveals that the protein relaxation is slower than the most rapid phase of NO recombination. Since protein relaxation in the distal pocket results in trapping of the photolyzed NO, the decrease in protein relaxation rate will slow the trapping of photolyzed NO ligands.[68,69] The consequence is that a greater fraction of NO molecules can recombine by the rapid pathway. In DHP−NO the trend is toward slower protein relaxation rates (increasing τ_{22}) and therefore less trapping in the slower recombining geminate state (smaller A_{12}) with increasing glycerol concentration. This result is particularly pronounced in the comparison of the 90% glycerol/buffer sample where there is a significant decrease in relaxation rate and concomitantly in the population of the rapid geminate phase. In H64V MbNO the protein relaxation lifetime

(τ_{22}) is relatively constant within the errors of ±15%. Correspondingly, the change in the amplitude of the slow phase of recombination (A_{12}) is significantly smaller in H64V MbNO.

To understand the effect of glycerol on NO recombination in detail we must first identify the origin of the effect. In a previous study, it was noted that the effect of increasing glycerol concentration could be to either increase the solvent viscosity or dehydrate the protein. Dehydration is predominantly a surface effect that involves replacement of surface waters (or slightly penetrating waters) by glycerol. As such the effect of viscosity and water replacement both produce a slowing of protein dynamics. The internal viscosity of myoglobin has been determined to be 4 cP.[68] Therefore, when the solvent viscosity exceeds 4 cP there is a constraint on the motion of α-helices in the globin structure with respect to one another. A similar effect is expected for water replacement since bound glycerol can form hydrogen bonds to many more partners than a bound water molecule. Thus, the effect of glycerol is to retard the internal time scale for protein dynamics. This view is consistent with studies of protein relaxation using the Soret band or band III as a probe.[41,70−73] On the basis of these studies it is known that the overall effect of glycerol is to slow protein dynamics. The effect of protein dynamics on NO recombination can best be understood by comparison with CO since there is a great deal of structural information on CO trajectories following photolysis in myoglobin.

A number of experimental techniques have shown that in MbCO, at either ambient or cryogenic temperatures, the photodissociated CO molecules quickly move to a docking site that is within the distal pocket and quite near the heme group.[11,19,74−76] Numerous spectroscopic studies[19,71,72,77] and X-ray crystallographic studies[11,35,75,78−83] of cryogenically trapped intermediates and the temperature dependence of their rebinding processes have indicated the presence of structurally distinct populations of photolyzed CO, still within the protein. DHP−NO, H64V MbNO, SWMbNO, and HHMbNO can all be hypothesized to have an NO docking site that is occupied following photodissociation. However, there is no crystallographic structural evidence concerning the nature of photolyzed states for diatomic ligands other than CO. Low-temperature (<35 K) infrared spectroscopic studies have demonstrated the existence of two NO populations in horse skeletal muscle MbNO.[31] The biexpoenential NO recombination has been interpreted in terms of two rotamers (called B_1 and B_2 in analogy with a similar suggestion for CO[1]). Recent time-resolved infrared studies of MbNO have also shown the biphasic nature of the rebinding kinetics.[32] On the other hand, the available data for DHP-CO and H64V-CO indicate that there is a single conformation in the B state,[54,84] although DHP−NO and H64V MbNO also have biexponential kinetics. The absence of a spectroscopically observed splitting in the B bands does not necessarily mean that there is only one rotamer or conformation of CO in the putative docking site but rather that the rotamers are not distinguishable by infrared spectroscopy. We recently considered the role of hydrogen bonding in producing the splitting of the B band into two bands (B_1 and B_2).[54] In that study, infrared experiments and DFT calculations were consistent with significantly stronger hydrogen bonding of CO to distal histidine (wild type) than to distal valine (H64V). Thus, it is expected that the two rotamers (CO and OC) will have a significant splitting in the presence of the imidazole ring (histidine side) and little or no splitting in the presence of valine. The appearance of two rotamers of CO arises following protein relaxation in the distal pocket. This can be seen most clearly in the picosecond infrared experiments where the anisotropy of the two B states arises on a ∼10 ps time scale associated with protein relaxation in horse skeletal muscle MbNO at room temperature.[74,76,85,86] The time scale for CO trapping can also be monitored by shifts in band III,[87] which are associated with Soret band shift.[70,88,89] Thus, the slow phase of the Soret band shift (τ_{22}) monitors conformational relaxation in the distal pocket that leads to trapping of bound diatomic ligands. This trapping is strongly dependent on solvent viscosity and the hydration state of the protein.

SCHEME 1: Sequential Kinetic Scheme for Biphasic NO Recombination[a]

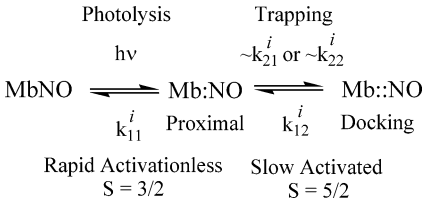

[a] The intrinsic rate constants k_{21}^i and k_{22}^i represent the nonexponential protein relaxation and are dependent on the solvent viscosity and protein hydration. The yield of formation of the proximal (Mb:NO) and docking (Mb::NO) states is dependent upon the spin state distribution, excess energy, and rate of protein relaxation.

The spin-dependent model for diatomic ligand recombination[23] is consistent with two channels for NO recombination, which results in biphasic recombination kinetics. According to the spin-dependent model the recombination of different spin states of photolyzed states is correlated with the distance of the ligand from the iron since the curve crossings for the $S = 5/2$ and 3/2 states, respectively, with the $S = 1/2$ ground state occurs at different distances from the heme iron. The partitioning of the spin states depends on the statistical distribution of spin states[23] and the ligand trajectory in the distal pocket, which may depend on excess energy of photolysis, temperature,[30] and protein relaxation rate. In the absence of protein constraints one-half of the NO ligands have the appropriate spin to recombine by the 3/2 → 1/2 pathway. This geminate pathway (τ_{11}) is ultrafast because the spin 3/2 state is a bound state. This means that there is no barrier for recombination from this state. This situation has also been called the harpoon mechanism.[30] We suggested elsewhere[23] that the hextet ($S = 5/2$) state recombines in a sequential mechanism as shown in Scheme 1. The intrinsic recombination rate constants k^i_{11} and k^i_{12} are approximately equal to the observed rate constants, k_{11} and k_{12}, as shown in the Supporting Information. The rate scheme is consistent with biexponential recombination kinetics with a nonexponential protein relaxation process that leads to trapping in the docking site. The nonexponential process described here has with two phenomenological rate constants, k_{21} and k_{22}. On a relatively short time scale, dictated by the geometry of the distal pocket and relaxation dynamics, approximately 50% of the NO ligands are trapped in the docking site Mb::NO and 50% are in the proximal Mb:NO site, from which they can recombine with the shorter time constant, τ_{11}. These considerations explain the observation of a rapid ($\tau_{11} \approx 9$ ps) time constant for NO recombination and a slower phase ($\tau_{12} \approx 52$ ps) for DHP−NO. According to this mechanism the 5/2 → 3/2 transition is rate limiting for the slower process (τ_{12}). The fact that the transition out of the docking site depends on temperature and viscosity is consistent with the hypothesis here that the trapping well depth depends on the strength of specific interactions of the NO ligand with amino acid that is closest to the docking site. The different distal pockets of different globins have a large effect on the

time constant of the slower rebinding process (τ_{12} which varies from ~52 ps in DHP−NO to 310 ps in HHMbNO). The difference in these proteins could be simply an effect of reduced trapping efficiency in the docking (i.e., reduced hydrogen-bond strength between the distal valine and NO compared to distal histidine and NO). The role of protein dynamics in the distal pocket is to alter the partitioning between the fast and slow channels. Since the time spent in the transition region can affect curve crossings, protein relaxation dynamics must play a role in determining the partitioning among these two channels (A_{11} and A_{12}). Given that the protein relaxation in the distal pocket depends on the glycerol concentration, this parameter can affect the partitioning as well as seen in trends in the data from three heme proteins, DHP−NO, H64V MbNO, and HHMbNO.

Although we can intuitively state that interaction of a C−H···NO is much weaker than Im−H···NO, the DFT results provide a quantitative estimate of the relative interaction potentials for valine and histidine with NO. The DFT calculations shown in Figure 7 support the hypothesis that the relative rate of NO rebinding depends on the magnitude of the stabilization of photolyzed NO in the distal pocket. Figure 7 shows that the interaction potential energy for NO with imidazole is ~3 kJ/mol for the Nϵ−H···NO rotamer, which is significantly stronger than the interaction potential with CH_4 (<1 kJ/mol). Note that 3 kJ/mol as the binding energy of NO in the binding site agrees with the experimentally determined activation energy for recombination by the slower process.[30] The large difference in the interaction strength for the two rotamers of NO (Nϵ−H···NO and Nϵ−H···ON) is consistent with FTIR data on the Mb−NO photoproduct obtained at cryogenic temperature.[31] On the other hand, the interaction of NO with valine (modeled using methane as the side chain) is much weaker with essentially no orientation dependence of the NO. Similar conclusions were reached for CO in the docking site.[54] For DHP and H64V Mb, the more rapid recombination kinetics compared to wild-type myoglobin are consistent with a smaller stabilization of NO in the distal pocket, which arises from the weaker interaction of NO with valine relative to the interaction with histidine. Weaker binding in the docking site of a hydrophobic distal pocket results in less stabilization following conformational relaxation in the distal pocket. The greatest effect of the weaker interaction (i.e., weaker hydrogen bonding) is observed for the slower process. Thus, the common feature in DHP−NO and H64V MbNO that both have a valine as the closest amino acid to bound NO also appears to play a role in the trajectory of photolyzed NO in both proteins.

Strong interactions on the proximal side, such as the strong hydrogen bond in DHP between the carbonyl group of L83 and the Nδ−H of the proximal histidine (H89),[4] do not have a large effect on NO recombination kinetics. In typical peroxidases the hydrogen-bonding interaction of the proximal histidine involves a Nδ−H···$^{-}$OOC interaction of the proximal histidine with aspartate.[90−92] The negative charge from the aspartate results in a charge relay that strengthens the Fe−His bond and supports high oxidation states of iron required for peroxidase function.[92,93] DFT calculations have shown that similar electronic interactions from a strong carbonyl hydrogen bond may play a role in increasing the charge density on the heme iron in DHP.[94] The greater peroxidase activity of DHP requires a charge relay of some kind. Nonetheless, the observations of similar NO rebinding rates in DHP−NO and H64V MbNO suggest that the proximal ligation effect plays a minor role in controlling NO ligand rebinding.

Conclusions

It is remarkable that a 1.5 Å shift in position of the active site of DHP shown in Figure 1 can change the nature of ligand interactions in the distal pocket to such a large extent. In myoglobin the closest distal amino acid to the heme iron is histidine 64 (H64). In DHP the closest side chain is valine 59 (V59) due to the 1.5 Å shift that places H55 further from the heme. Moreover, H55 in DHP is in equilibrium with a solvent-exposed conformation even at neutral pH.[4] Thus, the distal pocket of DHP is much more hydrophobic than that of any native myoglobin. NO dynamics can be used as a probe of dynamics interactions of diatomic ligands with the distal histidine (H55). The present study of distal pocket effects on the recombination of NO in DHP in various glycerol concentrations indicates that H55 in DHP does not interact strongly with photolyzed NO. As observed in HHMbNO, horse skeletal MbNO, and SWMbNO, the photodissociated ligand is found to partition into two populations that exhibit different rebinding kinetics. Solution glycerol content changes the relative amplitude of these two populations, favoring the more rapid process. The rapid process ($\tau_{11} \approx 9-11$ ps) is attributed to recombination by means of the $S = 3/2$ spin manifold. The rate constant of this rapid process is largely independent of the environment since both experiment and theory indicate that the process is activationless.[23,30] The slower process ($\tau_{12} \approx 50-90$ ps) is attributed to localization in a docking site with a barrier to recombination arising from the $S = 5/2$ manifold. The partitioning between the two spin channels can be affected by interactions in the distal pocket since proximity to the heme iron will increase curve crossing probabilities for spin transitions back to the lowest spin state required for bonding. Thus, the factors that affect partitioning among the two channels are excess energy of photolysis, temperature, and viscosity, all of which affect the dynamic energy balance between the ligand and the protein. Increasing glycerol concentration tends to favor the fast process by freezing out protein relaxation and preventing NO trapping in the docking site. The specific interaction with amino acid side chains in the docking site will affect the barrier for recombination and thus the time constant for the slow process. The interaction energy of NO with valine as the nearest residue is weaker than when histidine is the closest residue to NO. We hypothesize that the weaker interaction leads to a smaller barrier for recombination from the docking site and therefore a faster rate for the valine interaction than for histidine interaction. While the surface constraints due to viscosity and hydration state are communicated to the distal pocket in a similar manner for the globin−peroxidase DHP−NO and MbNOs, the overall kinetics are more rapid in DHP−NO, indicative of weak interactions of photolyzed NO in the distal pocket. These results are consistent with weaker hydrogen bonding observed in cryogenic DHP−CO vibrational studies[83] and the equilibrium solvent-exposed conformation of H55 in the X-ray structure.[4] The hydrophobic character of the distal pocket is remarkable given the fact that DHP is the first globin that also has native peroxidase function.

Acknowledgment. S.F. acknowledges support through NSF MCB-9874895. A.J. was the recipient of a long-term fellowship from the European Molecular Biology Organization.

Supporting Information Available: Basis set description, structures of calculated model systems, tables of relevant hydrogen-bonding, description of singular value decomposition, and figures showing SVD time courses and basis spectra. This

material is available free of charge via the Internet at http://pubs.acs.org.

References and Notes

(1) Shreve, A. P.; Franzen, S.; Simpson, M. C.; Dyer, R. B. *J. Phys. Chem. B* **1999**, *103*, 7969.

(2) Belyea, J.; Gilvey, L. B.; Davis, M. F.; Godek, M.; Sit, T. L.; Lommel, S. A.; Franzen, S. *Biochemistry* **2005** *44*, 15637.

(3) Franzen, S.; Dyer, R. B.; Woodruff, W. H.; Roach, M. R.; Chen, Y. P.; Dawson, J. H. *J. Am. Chem. Soc.* **1998**, *120*, 4658.

(4) Lebioda, L.; LaCount, M. W.; Zhang, E.; Chen, Y. P.; Han, K.; Whitton, M. M.; Lincoln, D. E.; Woodin, S. A. *Nature* **1999**, *401*, 445.

(5) LaCount, M. W.; Zhang, E. L.; Chen, Y. P.; Han, K. P.; Whitton, M. M.; Lincoln, D. E.; Woodin, S. A.; Lebioda, L. *J. Biol. Chem.* **2000**, *275*, 18712.

(6) Akiyama, K.; Fukuda, M.; Koboyashi, N.; Matsuoka, A.; Shikama, K. *Biochim. Biophys. Acta*−*Prot. Struct. Mol. Enzymol.* **1994**, *1208*, 306.

(7) Yang, F.; Phillips, G. N., Jr. *J. Mol. Biol.* **1996**, *256*, 762.

(8) Morikis, D.; Champion, P. M.; Springer, B. A.; Sligar, S. G. *Biochemistry* **1989**, *28*, 4791.

(9) Tian, W. D.; Sage, J. T.; Champion, P. M. *J. Mol. Biol.* **1993**, *233*, 155.

(10) Mourant, J. R.; Braunstein, D. P.; Chu, K.; Frauenfelder, H.; Nienhaus, G. U.; Ormos, P.; Young, R. D. *Biophys. J.* **1993**, *65*, 1496.

(11) Schlichting, I.; Berendzen, J.; Phillips, G. N., Jr.; Sweet, R. M. *Nature* **1994**, *371*, 808.

(12) Kachlova, G. S.; Popov, A. N.; Bartunik, H. D. *Science* **1999**, *284*, 473.

(13) Pilet, E.; Nitschke, W.; Rappaport, F.; Soulimane, T.; Lambry, J.-C.; Liebl, U.; Vos, M. H. *Biochemistry* **2004**, *43*, 14118.

(14) Négrerie, M.; Berka, V.; Vos, M. H.; Liebl, U.; Lambry, J.-C.; Tsai, A.-L.; Martin, J.-L. *J. Biol Chem.* **1999**, *274*, 24694.

(15) Négrerie, M.; Bouzhir-Sima, L.; Martin, J.-L.; Liebl, U. *J. Biol. Chem.* **2001**, *276*, 46815.

(16) Smerdon, S. J.; Krzywda, S.; Brzozowski, A. M.; Davies, G. J.; Wilkinson, A. J.; Brancaccio, A.; Cutruzzola, F.; Allocatelli, C. T.; Brunori, M.; Li, T.; et al. *Biochemistry* **1995**, *34*, 8715.

(17) Findsen, E. W.; Ondrias, M. R. *Photochem. Photobiol.* **1990**, *51*, 741.

(18) Springer, B. A.; Sligar, S. G.; Olson, J. S.; Phillips, G. N. *Chem. Rev.* **1994**, *94*, 699.

(19) Ansari, A.; Berendzen, J.; Braunstein, D.; Cowen, B. R.; Frauenfelder, H.; Hong, M. K.; Iben, I. E. T.; Johnson, J. B.; Ormos, P.; Sauke, T. B.; Scholl, R.; Schulte, A.; Steinbach, P. J.; Vittitow, J.; Young, R. D. *Biophys. Chem.* **1987**, *26*, 337.

(20) Henry, E. R.; Sommer, J. H.; Hofrichter, J.; Eaton, W. A. *J. Mol. Biol.* **1983**, *166*, 443.

(21) Franzen, S. *J. Am. Chem. Soc.* **2002**, *124*, 13271.

(22) Olson, J. S.; Phillips, G. N., Jr. *J. Biol. Inorg. Chem.* **1997**, *2*, 544.

(23) Franzen, S. *Proc. Natl. Acad. Sci. U.S.A.* **2002**, *99*, 16754.

(24) Carver, T. E.; Brantley, R. E., Jr.; Singleton, E. W.; Arduini, R. M.; Quillin, M. L.; Phillips, G. N., Jr.; Olson, J. S. *J. Biol. Chem.* **1992**, *267*, 14443.

(25) Ye, X.; Demidov, A.; Champion, P. M. *J. Am. Chem. Soc.* **2002**, *124*, 5914.

(26) Petrich, J. W.; Martin, J.-L.; Houde, D.; Poyart, C.; Orszag, A. *Biochemistry* **1987**, *26*, 7914.

(27) Petrich, J. W.; Lambry, J. C.; Balasubramanian, S.; Lambright, D. G.; Boxer, S. G.; Martin, J. L. *J. Mol. Biol.* **1994**, *238*, 437.

(28) Walda, K. N.; Liu, X. Y.; Sharma, V. S.; Magde, D. *Biochemistry* **1994**, *33*, 2198.

(29) Gibson, Q. H.; Regan, R.; Elber, R.; Olson, J. S.; Carver, T. E. *J. Biol. Chem.* **1992**, *267*, 22022.

(30) Ionascu, D.; Gruia, F.; Ye, X.; Yu, A. C.; Rosca, F.; Beck, C.; Demidov, A.; Olson, J. S.; Champion, P. M. *J. Am. Chem. Soc.* **2005**, *127*, 16921.

(31) Miller, L. M.; Pedraza, A. J.; Chance, M. R. *Biochemistry* **1997**, *36*, 12199.

(32) Kim, S.; Jin, G.; Lim, M. *J. Phys. Chem. B* **2004**, *108*, 20366.

(33) Petrich, J. W.; Poyart, C.; Martin, J. L. *Biochemistry* **1988**, *27*, 4049.

(34) Dantsker, D.; Roche, C.; Samuni, U.; Blouin, G.; Olson, J. S.; Friedman, J. M. *J. Biol. Chem.* **2005**, *280*, 38740.

(35) Schotte, F.; Lim, M. H.; Jackson, T. A.; Smirnov, A. V.; Soman, J.; Olson, J. S.; Phillips, G. N.; Wulff, M.; Anfinrud, P. A. *Science* **2003**, *300*, 1944.

(36) Li, T. S.; Quillin, M. L.; Phillips, G. N.; Olson, J. S. *Biochemistry* **1994**, *33*, 1433.

(37) Miner, C. S.; Dalton, N. N. *Glycerol*; Reinhold Publishing: New York, 1953.

(38) Sastry, G. M.; Agmon, N. *Biochemistry* **1997**, *36*, 7097.

(39) Martin, J.-L.; Vos, M. H. *Methods Enzymol.* **1994**, *232*, 416.

(40) MacFarlane, A. W., IV; Stanley, R. J. *Biochemistry* **2001**, *40*, 15203.

(41) Lambright, D. G.; Balasubramanian, S.; Boxer, S. G. *Chem. Phys.* **1991**, *158*, 249.

(42) Becke, A. D. *J. Chem. Phys.* **1997**, *107*, 8554.

(43) Lee, C. L.; Yang, W.; Parr, R. G. *Phys. Rev. B* **1988**, *37*, 785.

(44) Delley, B. *J. Chem. Phys.* **1990**, *92*, 508.

(45) Delley, B. *J. Chem. Phys.* **2000**, *113*, 7756.

(46) Mermin, D. *Phys. Rev. A* **1965**, *137*, 1441.

(47) Wood, P. M. *Biochim. Biophys. Acta* **1984**, *768*, 293.

(48) Cornelius, P. A.; Hochstrasser, R. M.; Steele, A. W. *J. Mol. Biol.* **1983**, *163*, 119.

(49) Kholodenko, Y.; Volk, M.; Gooding, E.; Hochstrasser, R. M. *Chem. Phys.* **2000**, *259*, 71.

(50) Franzen, S.; Kiger, L.; Poyart, C.; Martin, J. L. *Biophys. J.* **2001**, *80*, 2372.

(51) Chang, H. C.; Jiang, J. C.; Chuang, C. W.; Lin, S. H. *Chem. Phys. Lett.* **2004**, *397*, 205.

(52) Corey, E. J.; Lee, T. W. *Chem. Commun.* **2001**, 1321.

(53) Legon, A. C.; Lister, D. G.; Warner, H. E. *Angew. Chem., Int. Ed.* **1992**, *31*, 202.

(54) Nienhaus, K.; Olson, J. S.; Franzen, S.; Nienhaus, G. U. *J. Am. Chem. Soc.* **2005**, *127*, 40.

(55) Zhang, E.; Chen, Y. P.; Roach, M. P.; Lincoln, D. E.; et al. *Acta Crystallogr., D* **1996**, *52*, 1191.

(56) Carlson, M. L.; Regan, R.; Elber, R.; Li, H.; Phillips, G. N.; Olson, J. S.; Gibson, Q. H. *Biochemistry* **1994**, *33*, 10597.

(57) Rosca, F.; Kumar, A. T. N.; Ye, X.; Sjodin, T.; Demidov, A. A.; Champion, P. M. *J. Phys. Chem. A* **2000**, *104*, 4280.

(58) Zhu, L. Y.; Sage, J. T.; Champion, P. M. *Science* **1994**, *266*, 629.

(59) Kholodenko, Y.; Gooding, E. A.; Dou, Y.; Ikeda-Saito, M.; Hochstrasser, R. M. *Biochemistry* **1999**, *38*, 5918.

(60) Liebl, U.; Bouzhir-Sima, L.; Negrerie, M.; Martin, J. L.; Vos, M. H. *Proc. Natl. Acad. Sci. U.S.A.* **2002**, *99*, 12771.

(61) Slama-Schwok, A.; Negrerie, M.; Berka, V.; Lambry, J. C.; Tsai, A. L.; Vos, M. H.; Martin, J. L. *J. Biol. Chem.* **2002**, *277*, 7581.

(62) Chowdhury, P. K.; Kundu, S.; Halder, M.; Das, K.; Hargrove, M. S.; Petrich, J. W. *J. Phys. Chem. B* **2003**, *107*, 9122.

(63) Vos, M. H.; Lipowski, G.; Lambry, J. C.; Martin, J. L.; Liebl, U. *Biochemistry* **2001**, *40*, 7806.

(64) Gautier, C.; Negrerie, M.; Wang, Z. Q.; Lambry, J. C.; Stuehr, D. J.; Collin, F.; Martin, J. L.; Slama-Schwok, A. *J. Biol. Chem.* **2004**, *279*, 12000.

(65) Ye, X.; Yu, A. C.; Champion, P. M. *J. Am. Chem. Soc.* **2006**, *128*, 1444.

(66) Liebl, U.; Bouzhir-Sima, L.; Négrerie, M.; Martin, J.-L.; Vos, M. H. *Proc. Natl. Acad. Sci. U.S.A.* **2002**, *99*, 12771.

(67) Liebl, U.; Bouzhir-Sima, L.; Kiger, L.; Marden, M. C.; Lambry, J.-C.; Négrerie, M.; Vos, M. H. *Biochemistry* **2003**, *42*, 6527.

(68) Ansari, A.; Jones, C. M.; Henry, E. R.; Hofrichter, J.; Eaton, W. A. *Science* **1992**, *256*, 1796.

(69) Ansari, A.; Jones, C. M.; Henry, E. R.; Hofrichter, J.; Eaton, W. A. *Biochemistry* **1994**, *33*, 5128.

(70) Franzen, S.; Boxer, S. G. *J. Biol. Chem.* **1997**, *272*, 9655.

(71) Srajer, V.; Reinisch, L.; Champion, P. M. *J. Am. Chem. Soc.* **1988**, *110*, 6656.

(72) Chavez, M. D.; Courtney, S. H.; Chance, M. R.; Kuila, D.; Nocek, J.; Hoffman, B. M.; Friedman, J. M.; Ondrias, M. R. *Biochemistry* **1990**, *29*, 4844.

(73) Steinbach, P. J.; Ansari, A.; Berendzen, J.; Braunstein, D.; Chu, K.; Cowen, B. R.; Ehrenstein, D.; Frauenfelder, H.; Johnson, J. B.; Lamb, D. C.; Luck, S.; Mourant, J. R.; Nienhaus, G. U.; Ormos, P.; Philipp, R.; Xie, A.; Young, R. D. *Biochemistry* **1991**, *30*, 3988.

(74) Lim, M.; Jackson, T. A.; Anfinrud, P. A. *J. Chem. Phys.* **1995**, *102*, 4355.

(75) Srajer, V.; Teng, T. Y.; Ursby, T.; Pradervand, C.; Ren, Z.; Adachi, S.; Schildkamp, W.; Bourgeois, D.; Wulff, M.; Moffat, K. *Science* **1996**, *274*, 1726.

(76) Lim, M. H.; Jackson, T. A.; Anfinrud, P. A. *Nat. Struct. Biol.* **1997**, *4*, 209.

(77) Srajer, V.; Champion, P. M. *Biochemistry* **1991**, *30*, 7390.

(78) Teng, T.-Y.; Srajer, V.; Moffat, K. *Nat. Struct. Biol.* **1994**, *1*, 701.

(79) Engler, N.; Ostermann, A.; Gassmann, A.; Lamb, D. C.; Prusakov, V. E.; Schott, J.; Schweitzer-Stenner, R.; Parak, F. G. *Biophys. J.* **2000**, *78*, 2081.

(80) Chu, K.; Vojtchovsky, J.; McMahon, B. H.; Sweet, R. M.; Berendzen, J.; Schlichting, I. *Nature* **2000**, *403*, 921.

(81) Brunori, M.; Vallone, B.; Cutruzzola, F.; Travaglini-Allocatelli, C.; Berendzen, J.; Chu, K.; Sweet, R. M.; Schlichting, I. *Proc. Natl. Acad. Sci. U.S.A.* **2000**, *97*, 2058.

(82) Hummer, G.; Schotte, F.; Anfinrud, P. A. *Proc. Natl. Acad. Sci. U.S.A.* **2004**, *101*, 15330.

(83) Srajer, V.; Ren, Z.; Teng, T. Y.; Schmidt, M.; Ursby, T.; Bourgeois, D.; Pradervand, C.; Schildkamp, W.; Wulff, M.; Moffat, K. *Biochemistry* **2001**, *40*, 13802.

(84) Nienhaus, K.; Deng, P.; Belyea, J.; Franzen, S.; Nienhaus, G. U. *Biochemistry*, in press.

(85) Lim, M.; Jackson, T. A.; Anfinrud, P. A. *Proc. Natl. Acad. Sci. U.S.A.* **1993**, *90*, 5801.

(86) Lim, M.; Jackson, T. A.; Anfinrud, P. A. *Science* **1995**, *269*, 962.

(87) Jackson, T. A.; Lim, M.; Anfinrud, P. A. *Chem. Phys.* **1994**, *180*, 131.

(88) Franzen, S.; Morre, L. J.; Woodruff, W. H.; Boxer, S. G. *J. Am. Chem. Soc.* **1981**, *103*, 3070.

(89) Franzen, S.; Wallace-Williams, S. E.; Shreve, A. P. *J. Am. Chem. Soc.* **2002**, *124*, 7146.

(90) Poulos, T. L.; Kraut, J. *J. Biol. Chem.* **1980**, *255*, 575.

(91) Gajhede, M.; Schuller, D. J.; Henriksen, A.; Smith, A. T.; Poulos, T. L. *Nat. Struct. Biol.* **1997**, *4*, 1032.

(92) Goodin, D. B.; McRee, D. E. *Biochemistry* **1993**, *32*, 3313.

(93) Spiro, T. G.; Smulevich, G.; Su, C. *Biochemistry* **1990**, *29*, 4497.

(94) Franzen, S. *J. Am. Chem. Soc.* **2001**, *123*, 12578.

(95) Vojtechovsky, J.; Chu, K.; Berendzen, J.; Sweet, R. M.; Schlichting, I. *Biophys. J.* **1999**, *77*, 2153.